Journal of Solid State Chemistry 187 (2012) 7–14

Contents lists available at SciVerse ScienceDirect

Journal of Solid State Chemistry

journal homepage: www.elsevier.com/locate/jssc

The first 3D malonate bridged copper $[Cu(O_2C–CH_2–CO_2H)_2 \cdot 2H_2O]$: Structure, properties and electronic structure

A. Seguatni [a,*], M. Fakhfakh [b,c], L.S. Smiri [b], P. Gressier [d], F. Boucher [d], N. Jouini [c]

[a] LBPC-INSERM U 698, Institut Galilée, Université Paris XIII, 99, avenue J. B. Clément 93430, Villetaneuse, France
[b] Unité de recherche UR 12-30, Synthèse et Structure de Matériaux Inorganiques, Faculté des Sciences de Bizerte, 7021 Zarzouna, Tunisia
[c] Département de Chimie, Université du Québec à Montréal, C.P. 8888, Succ. Centre-ville, Montréal, Que., Canada H3C 3P8
[d] Institut des Matériaux Jean Rouxel, Université de Nantes, CNRS, 2 rue de la Houssinière, BP 32229, 44322 Nantes Cedex 3, France

ARTICLE INFO

Article history:
Received 7 July 2011
Received in revised form
2 November 2011
Accepted 26 November 2011
Available online 13 December 2011

Keywords:
Copper
Hybrid material
Structure
Magnetism
DFT calculation
GGA+*U*

ABSTRACT

A new inorganic-organic compound $[Cu(O_2C–CH_2–CO_2H)_2 \cdot 2H_2O]$ ([Cumal]) was hydrothermally synthesized and characterized by IR spectroscopy, thermal analysis and single crystal X-ray diffraction. [Cumal] is the first three-dimensional compound existing in the system Cu(II)–malonic acid–H_2O. Its framework is built up through carboxyl bridged copper where CuO_6 octahedra are elongated with an almost D_{4h} symmetry (4+2) due to the Jahn–Teller effect. The magnetic properties were studied by measuring its magnetic susceptibility in the temperature range of 2–300 K indicating the existence of weak ferromagnetic interactions. The electronic structure of [Cumal] was calculated within the density functional theory (DFT) framework. Structural features are well reproduced using DFT structural optimizations and the optical spectra, calculated within the dielectric formalism, explain very well the light blue colour of the compound. It is shown that a GGA+U approach with a U_{eff} value of about 6 eV is necessary for a better correlation with the experiment.

1. Introduction

In the last decade, numerous works have been carried out using the hydrothermal or solvothermal route to prepare new organic–inorganic materials. Several functionalized organic molecules namely diphosphonate or dicarboxylate have been used in these syntheses, leading to various structural types.

As far as considered, the dicarboxylate anions act as bridging ligands and ensure connection between 0D, 1D or 2D inorganic parts. This connection involves the two carboxylate groups, each group being linked to one inorganic part [1]. Thus the length of the dicarboxylic alkyl chain plays an important role in the separation of the inorganic parts. It confers its open character to the material [1–5].

It is interesting to note that, up to now, two compounds have been reported in the system Cu (II)–malonic acid–H_2O, with one deprotonated carboxylate group. The first one can be considered as formed by isolated $Cu(H_2O)_2(O_2C–CH_2–CO_2H)_2$ units held together by hydrogen bonds [6]. The second one $Cu(O_2C–CH_2–CO_2H)_2$ presents a two-dimensional structure with layers held together via hydrogen bonds [6].

In this paper we report on structure and characterization of the first 3D compound [Cumal] that has been identified in this system. This 3D network presenting a diamond-like structure is achieved via only one carboxylate group of the malonic acid, while the second one remains protonated and has no direct role in the connection between copper metallic center. The existence of such different dimensionalities (0D, 2D and 3D) for compounds with almost identical formula will be discussed.

In order to better understand the physical properties of this new 3D compound, electronic structure calculations were performed within the framework of the density functional theory (DFT). It will be shown that a GGA+*U* [7] approximation with a U_{eff} value close to 6 eV is needed to correctly reproduce the optical absorption spectra and consequently explain the light blue colour of the compound.

2. Experimental and computational Details

2.1. Preparation

The title compound was prepared under autogenous pressure, using the hydrothermal route starting from $CuCO_3$, $HO_2C(CH_2)CO_2H$ and H_2O introduced, in the molar ratio of 1/4/160. First, copper carbonate (1 mmol) and malonic acid (4 mmol) were mixed in 2 ml

* Corresponding author at: LBPC-INSERM U 698, Institut Galilée, Université Paris XIII, 99, avenue J. B. Clément 93430, Villetaneuse, France. Fax: 33 149 40 30 83.
E-mail address: seguatni@gmail.com (A. Seguatni).

0022-4596/$ - see front matter © 2011 Elsevier Inc. All rights reserved.
doi:10.1016/j.jssc.2011.11.044

of H_2O. The mixture was introduced in Teflon lined digestion bombs (measured pH=4.7) and heated at 453 K, over 3 days. The reaction product was filtered and washed with ethanol, then dried in an oven at 323 K for several hours. After fixing the pH at a value less than the pKa2 (5.7) of malonic acid, only one carboxylic acid group was deprotonated. This resulted in a compound with the chemical formula $[Cu(O_2C–CH_2–CO_2H)_2 \cdot 2H_2O]$.

2.2. Infrared spectroscopy

Infrared (I.R.) absorption analysis was carried out on the Paragon 1000PC Perkin-Elmer FTIR spectrometer in the range of 700–4000 cm^{-1} wave numbers (0.0869–0.4965 eV), with 5 scans and 4.0 cm^{-1} on a finely ground sample.

2.3. Thermal analysis

Thermal analysis was carried out under Argon flow, with a heating rate of 5 K min^{-1}, using a Setaram TG92 thermo-analyser.

2.4. Magnetic measurements

Variable-temperature susceptibility measurements were obtained for a powdered sample of [Cumal] on a SQUID magnetometer.

2.5. Diffuse reflectivity measurements

Spectrum was recorded on a finely ground sample with a Varian Cary 5G spectrometer equipped with a Harrick Praying Mantis accessory and the WinUV software for computer monitoring. The reflectance measurements were collected in the 200–3300 nm range (i.e. from 0.38 to 6.20 eV) with a mirror sample as the reference for 100% reflectance. From the observed reflectance (R), the Kubelka–Munk function ($K/S=((1-R)^2/(2R))$) was plotted versus energy in eV ((wavelength λ in nm) × (energy E in eV)=1239.9) to determine the band gap and absorption bands.

2.6. Structure determination

Diffraction intensities were collected at room temperature on a CAD4 with Mo $K\alpha$ radiation (λ=0.71073 Å). Analytical absorption corrections have been applied. Single crystal collected data were treated using the WINGX integrated system for windows programs [8] to undergo data reduction and intensity analysis. As the ONL test performed on a polycrystalline sample was positive, the noncentrosymmetric s.g. *Fdd*2 was retained for structure determination.

A structure solution was performed using the Patterson method [9], that provided copper and oxygen atoms locations. Then, refinements were carried out using the SHELXL 97 program [10], and subsequent Fourier syntheses gave the carbon atoms positions. The refinements of the atomic displacement parameters led to a significant decrease of the agreement factors R_1 and $WR_2(F^2)$. The resulting Fourier map gave the hydrogen atoms positions that were considered during the following refinements. Non-hydrogen atoms were refined anisotropically and isotropic displacement parameters were fixed at the value of 0.05 $Å^2$ for all hydrogen atoms. The crystallographic data and the refinement results are listed in Table 1. The atomic positions and atomic displacement parameters are listed in Table 2.

2.7. Electronic structure calculations

First-principles calculations were carried out within the framework of the density-functional theory (DFT) using the PBE variant of the generalized gradient approximation (GGA) for the exchange correlation-potential. Spin polarized calculation were considered to take into account the open shell nature for the copper atom (Cu^{II}). Whatever the starting magnetic configuration on the copper site, a $3d^9$ configuration is found at the end of the self consistent procedure. A Hubbard-like correction is introduced to improve the description of the localized strongly correlated copper 3*d* electrons. The effective on site Coulomb U_{eff} parameter was adjusted between 0 and 8 eV. The Projector Augmented Wave (PAW) method, as implemented in the Vienna Ab-initio Simulation Package (VASP), was used to treat the interaction of nuclei and core states with valence electrons. A 600 eV energy cut-off was found

Table 1
Crystallographic and experimental data.

Equipment	CAD-4 Enraf Nonius Diffractometer
Wave length	$\lambda(MoK\overline{\alpha})$=0.71073 Å
Chemical formula	$Cu(C_3H_3O_4)_2 \cdot 2H_2O$
Formula weight	305.68
Crystal system	Orthorhombic
a (Å)	13.873(4)
b (Å)	16.512(7)
c (Å)	9.137(3)
V(Å^3)	2093.1(13)
Z	8
Space group	*Fdd*2 (No. 43)
ρ (g cm^{-3})	1.940
μ (mm^{-1})	2.06
Number of collected data	2820
Number of independent data	1137
Number of independent data with $I>2\sigma(I)$	1102
$h\,k\,l$ limits for data collection	$-1 \le h \le 17;\ -1 \le k \le 20;\ -11 \le l \le 11$
Scan mode	ω–2θ
Recording range (deg.)	$2.94 < \theta < 26.97$
R(int)/R(sigma)	0.0061/0.0155
Number of parameters during refinements	95
Number of restraints	1
R_1/$WR_2(F^2)$/Goof_S	0.0309/0.0855/1.105
R_1 for 2360 data with $I>2\sigma(I)$	0.0323
Extinction parameter	0.2×10^{-3}

Table 2
Atomic positions and anisotropic displacement parameters.

	DRX			DFT		
Atom	***x/a***	***y/b***	***z/c***	***x/a***	***y/b***	***z/c***
Cu1	1/4	1/4	0.11384(8)	1/4	1/4	0.1059
O1	0.41477(17)	0.19067(13)	0.1128(3)	0.4026	0.1835	0.0984
O2	0.2117(2)	0.17563(15)	0.9588(3)	0.2008	0.1800	0.9546
C1	0.1944(2)	0.1001(2)	0.9698(4)	0.1841	0.1041	0.9591
C2	0.2122(2)	0.05611(16)	0.1129(4)	0.2037	0.0552	0.0988
H1	0.17660	0.00560	0.11100	0.2815	0.0407	0.0992
H2	0.28010	0.04270	0.11860	0.1643	0.9979	0.0943
C3	0.1846(2)	0.1016(2)	0.2507(4)	0.1858	0.0987	0.2408
O3	0.13781(12)	0.06473(10)	0.34800(16)	0.1485	0.0597	0.3518
O4	0.21210(16)	0.17401(8)	0.26863(19)	0.2077	0.1718	0.2597
OW	0.92978(12)	0.09860(12)	0.3579(2)	0.9063	0.0834	0.3527
HW1	0.92040	0.13630	0.45860	0.9039	0.1159	0.4451
HW2	0.89380	0.04280	0.36320	0.8959	0.1206	0.2702
H3	0.14100	0.09000	0.42510	0.1271	0.9965	0.3418
Atom	U_{11}	U_{22}	U_{33}	U_{12}	U_{13}	U_{23}
Cu1	0.03040	0.01087	0.01304	−0.00358	0.00000	0.00000
O1	0.03885	0.02007	0.01591	0.00727	−0.00027	0.00231
O2	0.04189	0.01388	0.01863	−0.00545	−0.00409	−0.00135
C1	0.01881	0.01647	0.01522	−0.00076	0.00041	−0.00080
C2	0.03179	0.01139	0.01712	−0.00096	−0.00016	−0.00157
C3	0.01998	0.01463	0.01327	0.00069	−0.00121	0.00113
O3	0.03231	0.01977	0.01991	−0.00660	0.00190	0.00061
O4	0.03840	0.01538	0.01599	−0.00471	0.00323	−0.00269
OW	0.04341	0.03401	0.03238	−0.00229	−0.00032	−0.00405

suitable to ensure the convergence of the plane-wave expansion for the wave function. For the DFT geometry optimization, a $2\times2\times2$ *k*-point grid (5 irreducible *k*-points) was used for the Brillouin zone integration. Optimization of all the atomic positions was performed by maintaining the experimental cell parameters and minimizing the forces down to the residual value of 0.05 eV/Å. The frequency dependant dielectric tensor was evaluated in a post-processing step using the optical option available in VASP [11]. The calculation was done at the Random Phase Approximation (RPA) level using a denser $(4\times4\times4)$ k-mesh (18 irreducible *k*-points) but without taking into account the local field effects. The cell shape was not allowed to relax, as significant deviations of the cell parameters are observed compared to experiment together with the deprotonation of the O3–H3 group (see supplementary data).

The as-obtained coordinates as well as interatomic distances are in fairly in good accordance with those inferred from X-ray diffraction. However, differences are observed for the H3 position which belongs to the carboxylate group, the water molecule orientation, and the hydrogen bond network (Tables 2 and 3).

Table 3
Selected geometric parameters (Å).

	DRX	DFT
Atoms 1,2	***d* 1,2 [Å]**	***d* 1,2 [Å]**
Cu1–O2	1.948(3)	1.937
Cu1–O4	1.962(3)	1.997
Cu1–O1	2.487(3)	2.386
O2–C1	1.275(5)	1.275
C1–C2	1.515(5)	1.535
C2–C3	1.515(5)	1.504
C2–H1	0.97	1.11
C2–H2	0.97	1.10
C3–O3	1.259(4)	1.308
C3–O4	1.264(4)	1.266
O3–H3	0.8200	1.089
OW–HW1	1.119	1.000
OW–HW2	1.049	0.983
OW–H3	2.833	1.402
OW–H3$^{(ii)}$	2.027	3.384
HW2–O3$^{(ii)}$	1.834	1.922
HW1–O1$^{(ii)}$	1.672	1.791

Symmetry codes: (i) $0.25+x$, $0.25-y$, $0.25+z$; (ii) $-0.25+x$, $0.25-y$, $-0.25+z$; (iii) $1-x$, $1-y$, z.

3. Structure description and comparison with other malonate-metal compounds

3.1. Structure description

The structure can be described as a three dimensional hybrid organic–inorganic framework built up of Cu(II) metal atoms coordinated by six oxygen atoms from malonate ligands. The asymmetric unit is constituted of one Cu(II) atom, one malonate ion ($HO_2C–CH_2–CO_2^-$) and one water molecule (Fig. 1a). As is shown in Fig. 1a, the two carboxylic acid groups play different roles. The deprotonated group (O1–C1–O2) acts as a bridging ligand whereas the protonated one (O3–C3–O4) is a unidentate ligand. All oxygen atoms in the CuO_6 octahedra result from four equivalent malonate anions: two equivalent oxygen atoms (O1, O1$^{(iii)}$) in trans positions at a distance of 2.487 Å and two pairs of equivalent oxygen atoms (O2, O2$^{(iii)}$) and (O4, O4$^{(iii)}$), which are at short bond distances ($\sim$1.95 Å), in cis positions (table 3). Thus the geometry of the copper ion can be described as distorted octahedral with the two axial bonds. These are greatly elongated as a result of the Jahn–Teller effect as currently encountered for copper compounds [12]. Two malonate anions are grafted to the copper atom via their farthest oxygen atoms O(2) and O(4), leading to two six-membered chelate rings, related by a symmetry axis (C_2) (Fig. 1b). The bridging character of the deprotonated carboxylic group (O1–C1–O2) allows copper ions to be connected to each other. Indeed each CuO_6 octahedron is connected via four bridging (O1–C1–O2) carboxyls to four other CuO_6 octahedra (Fig. 1b). According to Yaghi description of hybrid networks, this

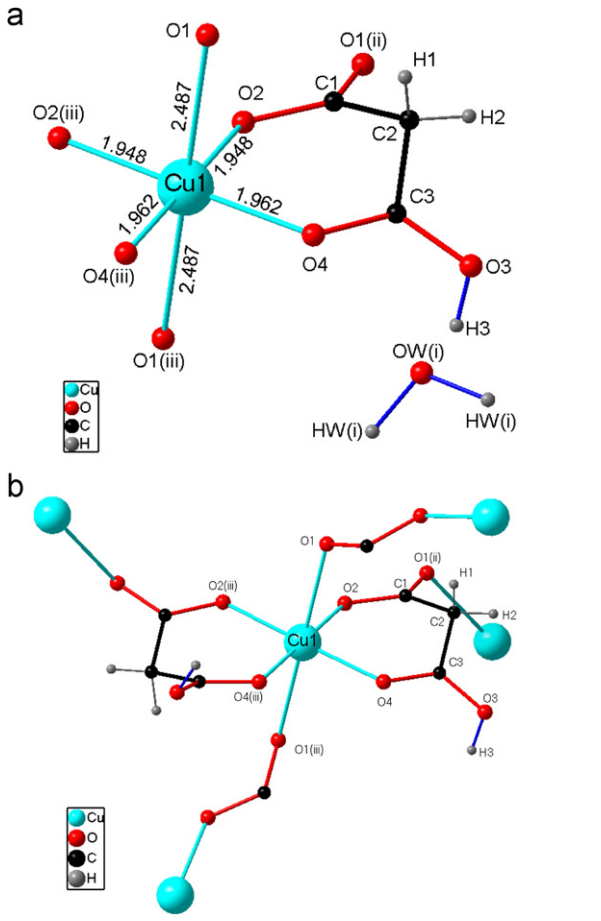

Fig. 1. (a) The asymmetric unit of [Cumal]. (b) Structural fragment of [Cumal] showing the copper connection via four bridging carboxyl groups.

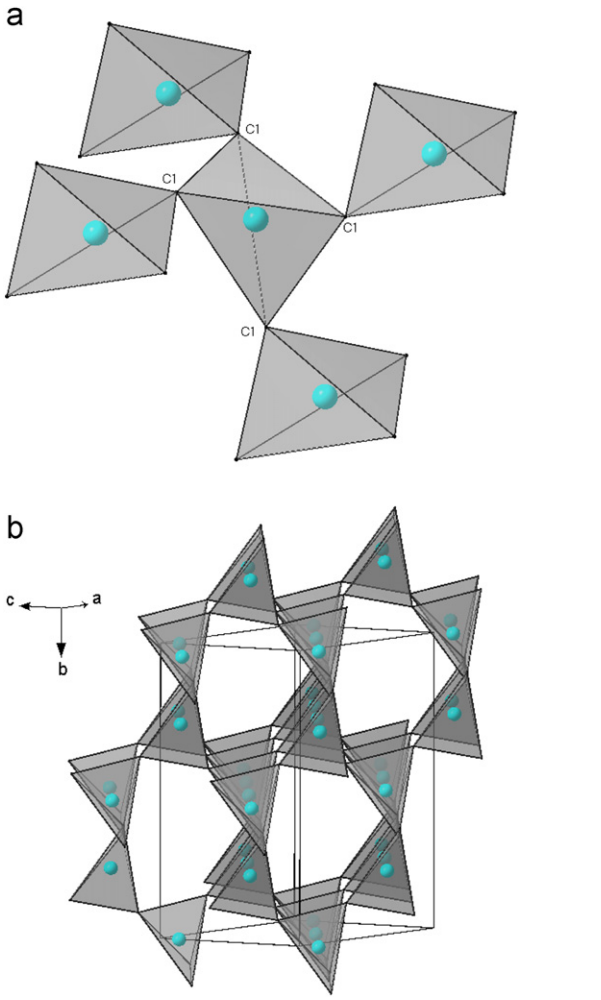

Fig. 2. (a) The CuC_4 tetrahedron sharing all its corners. (b) Details of the crystal structure of the title compound d viewed in [1 0 1] showing pseudo-hexagonal tunnels.

3D framework can be described as made up from deformed CuC_4 tetrahedron (terminating carbon around Cu:4C1) with common corners (Fig. 2a and b). Regardless of symmetry, this structure can be classified as an extended diamond structure [13] presenting pseudo-hexagonal tunnels.

X-ray refinements and DFT calculations show that the water molecules are confined in these tunnels and linked to carboxyl groups via strong hydrogen bonds. It should however be noted that the water molecule orientation and hydrogen bond network inferred from DFT differ slightly from that obtained by X-ray refinements (Fig. 3).

3.2. Comparison with other related malonate-metal compounds

One can note that the copper ion is grafted to two malonate anions via their oxygen atoms O(2) and O(4), resulting in two six-membered chelate rings, related by a symmetry axis (C_2). Regardless of the symmetry, it is important to note that such rings units have been often encountered in malonate-metal compounds where the malonic acid can be partially deprotonated: $Cu(HO_2CCH_2CO_2)_2$ [14] Cu $(H_2O)_2(HO_2CCH_2CO_2)_2$ [15] or totally deprotanated, $[M(H_2O)_2][M(O_2CCH_2CO_2)_2(H_2O)_2]$ (M=Co or Ni) [16], $[BaMn_{1-x}M_x(O_2CCH_2CO_2)2(H_2O)_4]$ (M=Fe, Co or Cu) [17], $[Cu(O_2CCH_2CO_2)_2(meaH)_2]$ with (*mea*=monoethanolammonium) [18] and $[M(H_2O)_6][Cu(O_2CCH_2CO_2)_2H_2O]$ (M=Mn, Co, Ni, Cu or Zn) [6]. Although such units can be considered as a building block from which all these structures were developed [14], the compounds cited above are different from [Cumal] on two points: (i) the symmetry of the two six membered ring units and (ii) the role of water molecules. Indeed, in all these compounds, the two six membered ring units present centrosymmetrical configuration with copper located at the inversion centre. Furthermore water molecules behave as strong nucleophilic ligands and thus belong to the first coordination sphere of the metal. Thus around the copper ion one can distinguish four almost planar oxygen atoms arising from carboxylate groups and two trans apical oxygen arising from water molecules (Fig. 1a). This is likely to be responsible of the low dimensionality of the as-obtained compounds since it allows the structure to be developed only in the six ring plane. This leads to structures constituted of independent (0D) [16] or bi-dimensional (2D) units [14–19], the cohesion of the framework being ensured via hydrogen bonds (Fig. 4).

Conversely, in [Cumal], the symmetry of the two six-membered rings is lowered. It becomes a C_{2v} one. The status of water molecules is different, as they behave as zeolitic species. In the absence of centre of symmetry the development of the structure is ensured through four carboxyl groups (O(1)C(1)O(2)), including (O(2), O(2)(iii)) pair of points in an average plane parallel to the two six-membered ring plane and (O(1), O(1)(iii)) pair of points in a perpendicular plane (Fig. 2a, b). These changes favour a three dimensional framework with tunnels where water molecules are located. To the best of our knowledge, [Cumal] is the first example of 3D structure with a covalent framework within the system Cu–Malonic acid–H_2O.

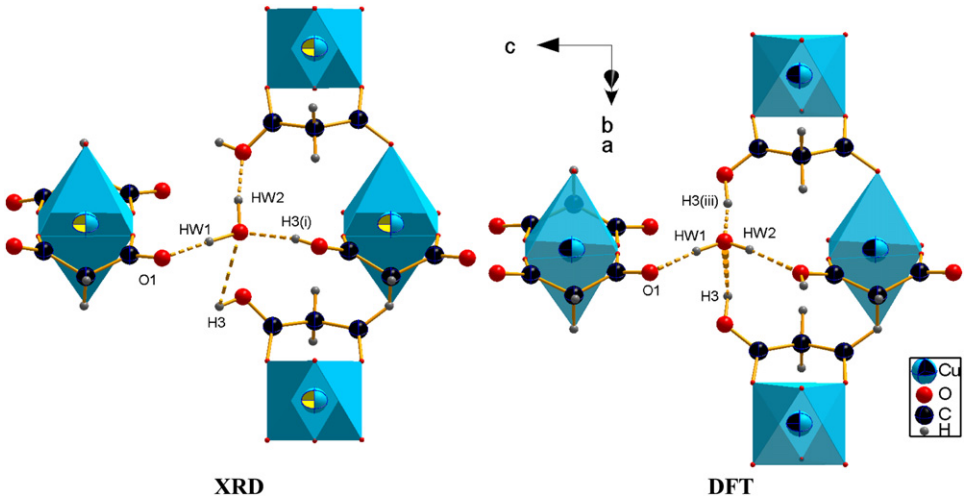

Fig. 3. Structural fragment of [Cumal] showing a network of hydrogen bonds. Hydrogen bonds determined by XRD and DFT.

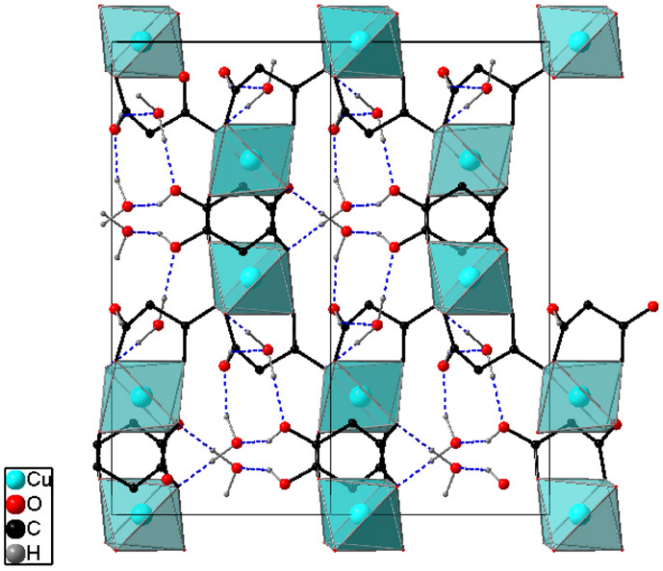

Fig. 4. [1 0 1] view of [Cumal] showing the hydrogen bonds in the unit cell.

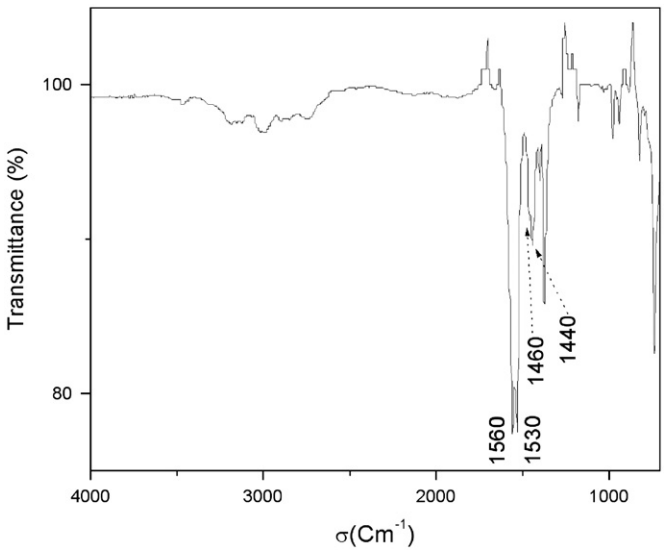

Fig. 5. Infrared spectrum of [Cumal].

Such different dimensionalities (0D, 2D and 3D) for compounds with almost identical formula appear to be closely related to the synthesis conditions. [Cumal] was obtained using hydrothermal method at 453 K whereas the cited compounds were prepared by slow evaporation at room temperature. As observed in several previous works, in comparison with conventional aqueous reactions, hydrothermal techniques cause reaction shifts from the thermodynamic to kinetic domain and thus facilitate the formation of higher-dimensional hybrid compounds [20–24].

4. Infrared spectroscopy

The infrared spectrum given in Fig. 5 shows absorption bands in three spectral regions characteristic of alkyl carboxylate hybrid materials. The bands observed in the region below 1400 cm^{-1} are related to ν(C–C) modes. Two sets of bands are observed, in the range between 1440 and 1560 cm^{-1}, which is in accordance with the existence of two different carboxyl groups revealed by the crystal structure analysis. The bands at 1460, 1440 cm^{-1} should be assigned to ν_s(C–O) while the second set at 1560, 1530 cm^{-1} should be assigned to ν_{as}(C–O). The crystal structure analysis showed that the (O3–C3–O4) carboxyl group can be considered as pseudo-bridging ligand because it is monodentate and involved in hydrogen bonding [25] whereas the carboxyl group (O1–C1–O2) has a strictly bridging character. According to Nakamoto rules, the $\Delta = \nu_{as}(C–O) - \nu_s(C–O)$ value of strictly bridging character should be lower than that for monodentate carboxylates [26]. Taking into account the structural features we can propose a precise assignment of the observed bands. The peak at 1560 cm^{-1} is attributed to the ν_{as}(C3–O) and the most intense in the first set of peaks should be assigned to the ν_s(C3–O). Thus, the peaks at 1530 cm^{-1} and 1460 cm^{-1} can be assigned to ν_{as}(C1–O) and ν_s(C1–O) ,respectively. This gives Δ values about 120 cm^{-1} and 70 cm^{-1} for (O3–C3–O4) and (O1–C1–O2), respectively. The assignment of this Δ values is in accordance with our previous work related to $[Cd(OH)]_2[O_2C(CH_2)_2CO_2]$ and $[Cd_3(OH)_2][O_2C(CH_2)_2CO_2]_2$ [27], based on symmetry carboxylate groups differentiation [25].

The spectral region around 2900 cm^{-1} is characteristic of vibrational modes ν(C–H) of $–CH_2–$ group within carbon chain.

The upper spectral range is reserved to ν(O–H) vibrational modes involving the water molecule or the carboxyl (O–H) group.

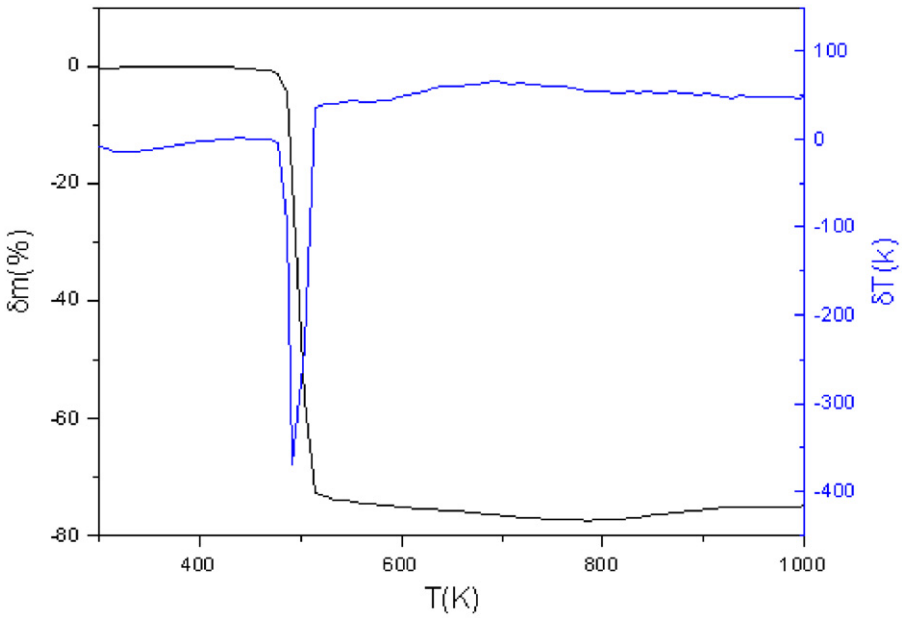

Fig. 6. TG–DTA curves of [Cumal].

5. Thermal behaviour

Thermogravimetric (TG) and differential thermal analysis (DTA) were obtained under argon for powder sample in the range of 308–1273 K (Fig. 6). TGA and DTA analyses reveal that the weight loss occurred in one step at 475 K. It leads to the final product CuO as confirmed by powder X-ray diffraction analysis. The experimental weight loss about 74% is in keeping with that calculated (73.9%). The DTA curve shows an endothermic peak which is understandable since the decomposition was conducted under argon flow. Although X-ray diffraction showed that the water molecules are located in tunnels and not directly linked to cation, the concomitant departure of water and carboxylate group can be explained by the strong hydrogen bonds between the water molecules located in the tunnels and the carboxylate groups of the framework as established by structural study. This leads us to conclude that most probably the water molecule plays an important role in the structure stabilization of the 3D framework, and explain why the isostructural 3D non-hydrated compound $Cu(O_2C–CH_2–CO_2H)_2$ is not stable. It exists only with a 2D framework, as discussed above.

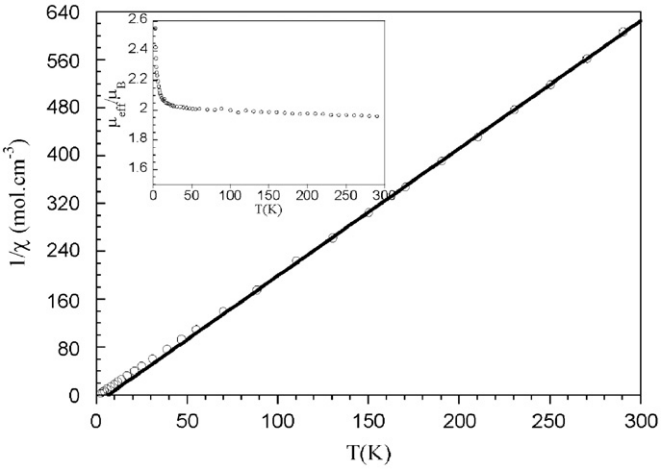

Fig. 7. The plots of $1/\chi_M$ (χ_M is variable temperature magnetic susceptibility under a magnetic field of 200 G) where circles stand for experimental data and continuous line for simulated curve with $1/\chi=(T-\theta)/C$ and the effective moment μ_{eff}/μ_{eff} versus T of [Cumal].

6. Magnetic behaviour

The variable temperature magnetic susceptibility data of [Cumal] were measured in the range of 2–300 K under a magnetic field of 200 G. The plots of $1/\chi_M$ and μ_{eff} versus T are given in (Fig. 7), where circles stand for experimental data and continuous line for simulated curve with $1/\chi=(T-\theta)/C$. At 300 K, χ_M is 1.58×10^{-3} cm^3 mol^{-1}, which corresponds to an effective moment of 1.95 μ_B. These values slightly higher than expected for uncoupled Cu(II) ions ($\chi_M=1.25\times10^{-3}$ cm^3 mol^{-1}, and $\mu_{eff}=1.73$ μ_B; for $g=2$) are in accordance with those observed in the literature for copper (II) compounds [28]. The plot of μ_{eff} versus T (Fig. 7) shows μ_{eff} to increase slightly on cooling to reach a value of 2.10 μ_B at 10 K, and to increase abruptly to attain 2.76 μ_B at 2 K. This behaviour indicates that there are weak ferromagnetic interactions at low temperature. The $1/\chi$ plot as a function of temperature follows Curie–Weiss law at high temperature (above 80 K) with $C=0.470(1)$ cm^3 mol^{-1} K and $\theta=6.5(5)$ K, which confirms the predominantly ferromagnetic interactions. Considering $\theta=zJS(S+1)/3K_B$ with $z=4$ (number of nearest neighbours around copper atom) gives $J/K_B=0.96$ K. Despite its three dimensional character, [Cumal] presents weak ferromagnetic behaviour very similar to that observed by Delgado et al. [16] in the case of $Cu(HO_2CCH_2CO_2)_2$ a 2D compound or by Yan et al. in the case of one-dimensional copper cyanide coordination polymer [28].

7. Electronic band structure calculation and analysis

To better investigate the [Cumal] compound, its electronic structure obtained from DFT calculation is now presented. Spin polarized calculation was considered with a ferromagnetic ordering between the copper sites. As expected from experiments, a d^9 configuration is found on the metal site with a local magnetic moment corresponding to one unpaired electron. The as-obtained electronic structure is presented in Fig. 8. Taking first the

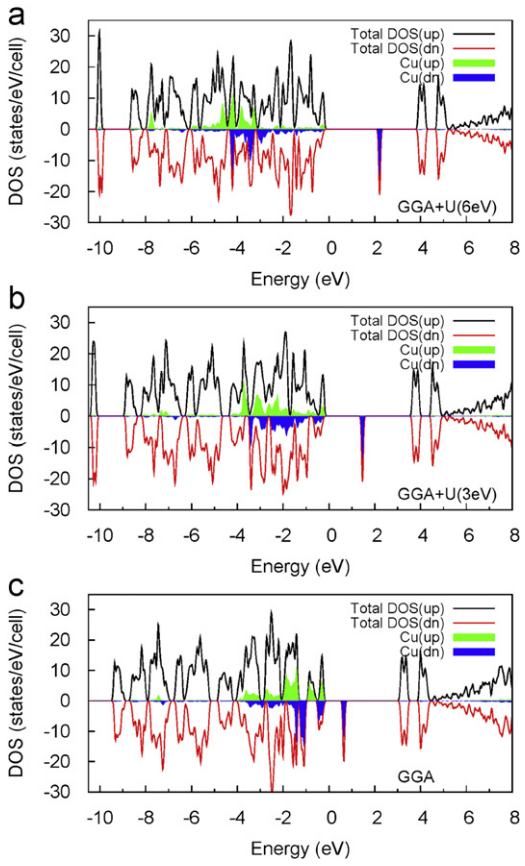

Fig. 8. Total and partial copper density of states (DOS) for the up and down spin channels and for a GGA calculation and two different GGA+U calculations (U_{eff}=3, 6 eV).

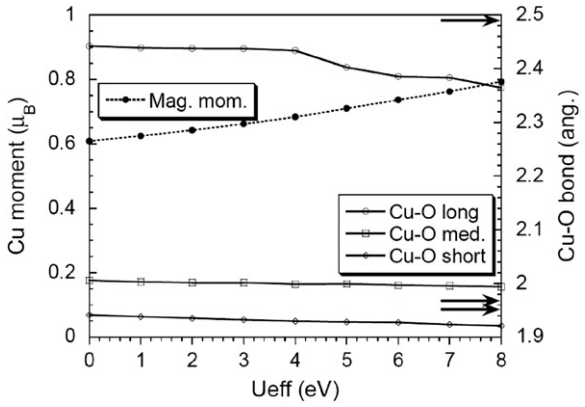

Fig. 9. Evolution of the local magnetic moment on the copper atom (left) and Cu–O bond lengths (right) as function of U_{eff} in GGA+U calculations.

standard GGA calculation (Fig. 8a), it is quite easy to identify the characteristic features of a strong Jahn–Teller distortion. On both spin channels, the (d_{xy}, d_{xz} and d_{yz}) orbitals within the [−4 eV, −1 eV] range are occupied and present some mixing with the oxygen p states. The distortion generates a splitting of the d_{x2-y2} and d_{z2} states, with both states being occupied for the spin up while the d_{x2-y2} is empty for the minority states. The gap between the HOMO and LUMO originates from those d bands. 3–4 eV above the Fermi level, the antibonding C–O and C–C molecular levels can be found, while the corresponding bonding states are found at the bottom of the valence band. The continuum (5 eV above E_F) arises from the 4s and 4p copper states. It is however known that GGA is not a good approximation for describing the correlation of the late transition metal elements. An effective U Coulomb parameter can be used in that case to improve the description of the 3d copper states. The U_{eff} parameter is however an empirical, thus more care is needed for a judicious choice [29]. The total and partial density of states obtained for two different U_{eff} values are shown in Fig. 8b,c. The picture described previously is clearly modified. While the empty d_{x2-y2} band moves higher in energy with the U value, the occupied d states are clearly pushed well below the Fermi level. The higher the U_{eff} is, the lower the d bands are. The HOMO is now mainly constituted with oxygen p states and that picture corresponds to what is called a charge transfer insulator.

For a correct estimation of U_{eff} value, we are looking for its effect on the Jahn–Teller distortion and on the local magnetic properties. The U_{eff} dependence of the three set Cu–O distances is shown in Fig. 9. One can see that the experimental structural distortion ($2\times1.947(2)$, $2\times1.964(3)$, $2\times2.489(2)$; arrows in Fig. 9) is rather well reproduced whatever the U_{eff} value (2×1.93, 2×1.99, 2×2.39 for a U_{eff}=6 eV). Likewise, no clear change is observed on the local magnetic moment on the copper site. Similarly to what is observed for cuprates by Blaha et al. [29], it increases steadily with the U_{eff} from 0.61 μ_B with the GGA to 0.79 μ_B with an 8 eV U_{eff} value.

At this stage, no evidence for a better U_{eff} value can be shown. In order to consolidate our analysis, diffuse reflectance measurements were performed on [Cumal] powder sample. Such an experiment is sensitive to absorption process and can give precise information on the optical transition from the valence to conduction bands. The calculated Kubelka–Munk function from the diffuse reflectance spectrum is shown in Fig. 10. It presents an absorption band in the near IR to red region (from 1 to 2 eV), in accordance with the light blue colour of [Cumal]. This band has a very particular shape that will greatly help us in determining the optimum U_{eff} value. The optical absorption process can be simulated by calculating the imaginary part of the microscopic dielectric tensor that comes directly from the transition matrix elements between the valence band and the conduction band. The as-obtained ε_2 is shown in Fig. 11 for the different U_{eff} values. The simulated spectrum obtained for the GGA is easily explained using the DOS and partial DOS pictures presented in Fig. 8. The two absorption bands observed at 1 eV and 2.5 eV correspond to transitions from the states at the top of the valence band to the bottom of the conduction band. Only the minority spin down

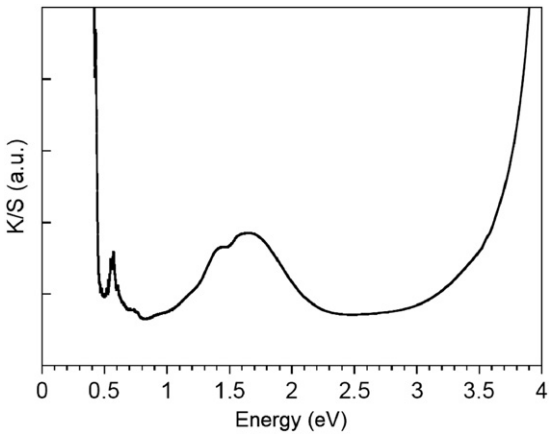

Fig. 10. UV–vis diffuse-reflectance spectrum of [Cumal] after application of the Kubelka–Munk transformation.

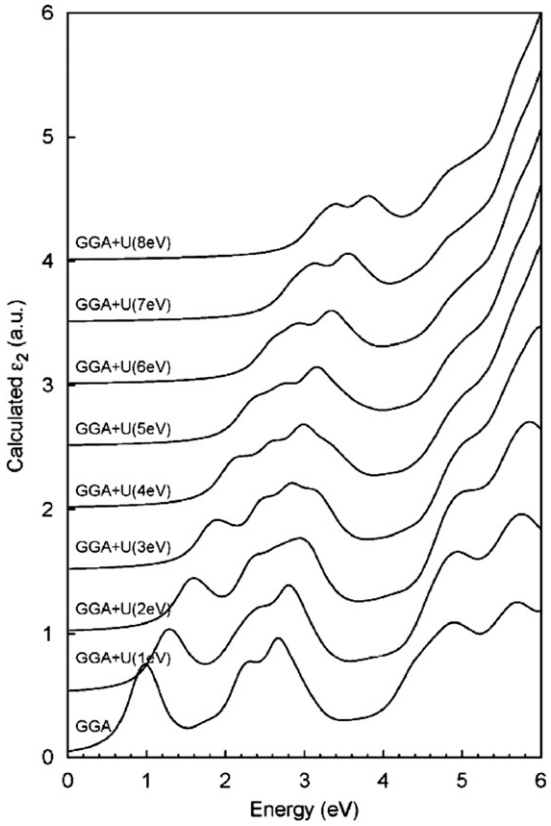

Fig. 11. DFT prediction of the imaginary part of the dielectric function of [Cumal] as a function of U_{eff} in the GGA+U calculations.

channel contributes to this absorption process. As shown by others [30], this absorption process obeys the permitted transition rules for the matrix elements i.e. the Cu d–d transition is not permitted. So, transitions come from oxygen p (or oxygen s) character at top of the valence band towards oxygen s (or oxygen p) states that are mixed with copper d states in the conduction band called the "d_{x2-y2}" band. Clearly, the calculated ε_2 spectrum for the GGA (Fig. 11) is very far from the observed absorption spectrum (Fig. 10). By increasing U_{eff}, a significant evolution of the absorption peak shape is obtained. One can note a shift at higher energy of the absorption peaks with a collapse of the two separated bands into a single one, as observed experimentally. It is clear that the 6 eV U_{eff} value leads to the greatest accordance between the calculated and observed absorption peak shape. Most probably, this U_{eff} value can be used to describe the electronic structure of other [Cumal] compounds. More generally, it seems to a fairly good value for Cu d^9 just as Blaha et al. [29] proposed a value close to 6 eV for Cu^{II} in cuprates, based on electric field gradient calculations. Surprisingly, Yao et al. [31] have presented electronic structure calculations on 3D coordination polymer $[Cu(mal)(DMF)]_n$ using only standard GGA calculations. Their band structure picture would probably be much different using the GGA+U method with our recommended U_{eff} value. Despite this calculation improvement, the GGA+U method presents some limitation as regards explaining the overall absorption spectrum. Indeed, the absorption peak is calculated roughly 1.3 eV, which is too high compared to experiment. This is a known limitation of the RPA. More sophisticated but time-consuming many body calculations would be necessary to improve this description. This is out of the scope of the present paper.

8. Supplementary material

Crystallographic data (excluding structure factors) for the structures reported in this paper have been deposited with the Cambridge Crystallographic Data Centre as supplementary publications No. CCDC (620497). Copies of the data can be obtained free of charge on application to CCDC, 12 Union Road, Cambridge CB21EZ, UK (fax: (+44) 1223-336-033; e-mail: deposit@ccdc.cam.ac.uk).

Acknowledgments

The authors would like to thank Patrick Aschehoug and Bruno Viana (Équipe ENSCP du Laboratoire de Chimie de la Matière Condensée de Paris) for supervising the ONL test experiment, Florian Massuyeau (IMN Nantes) for diffuse reflectivity measurements, Philippe Molinié (IMN Nantes) for magnetic measurements and J. Morrice-Abrioux (IUT Saint-Denis, Université Paris 13) for careful reading of the manuscript.

Appendix A. Supplementary Information

Supplementary data associated with this article can be found in the online version at doi:10.1016/j.jssc.2011.11.044.

References

[1] C. Mellot-Draznieks, G. Férey, Prog. Solid State Chem. 33 (2005) 187.
[2] M. Riou-Cavellec, C. Albinet, J.M. Grenèche, G. Férey, J. Mater. Chem. 11 (2001) 3166.
[3] O.K. Barthelet, C. Merlier, C. Serre, M. Riou-Cavellec, D. Riou, G. Férey, J. Mater. Chem. 12 (2002) 1132.
[4] D. Arcos, M. Vallet-Regí, J. Solid State Chem. 148 (1999) 376.
[5] M. Eddaoudi, J. Kim, M. O'Keeffe, O.M. Yaghi, J. Am. Chem. Soc. 124 (2002) 376.
[6] Y. Rodrıguez-Martın, M. Hernandez-Molina, F.S. Delgado, J. Pasan, C. Ruiz-Pérez, J. Sanchiz, F. Lloret, M. Julvec, CrystEngComm 4 (2002) 522.
[7] V.I. Anisimov, J. Zaanen, O.K. Andersen, Phys. Rev. B 44 (1991) 943.
[8] A.T.H. Lenstra, O.N. Kataeva, Acta Cryst. B57 (2001) 497.
[9] L.J. Farrugia, J. Appl. Crystallogr. 32 (1999) 467.
[10] G.M. Sheldrick, Z. Dauter, K.S. Wilson, H. Hope, L.C. Sieker, Acta Cryst. D 49 (1993) 18.
[11] M. Gajdos, K. Hummer, G. Kresse, J. Furthmuller, F. Bechstedt, Phys. Rev. B 73 (2006) 9.
[12] H.A. Jahn, E. Teller, Proc. R. Soc. A 161 (1937) 220.
[13] G.M. Sheldrick (Ed.), SHELXL-97, University of Goettingen, Germany, 1997.
[14] Y. Rodrıguez-Martın, J. Sanchiz, C. Ruiz-Pérez, F. Lloret, M. Julve, CrystEngComm 4 (2002) 631.
[15] F.S. Delgado, M. Hernandez-Molina, J. Sanchiz, C. Ruiz-Pérez, Y. Rodrıguez-Martın, T. Lopez, F. Lloret, M. Julve, CrystEngComm 6 (2004) 106.
[16] F.S. Delgado, J. Sanchiz, C. Ruiz-Pérez, F. Lloret, M. Julve, CrystEngComm 6 (2004) 443.
[17] I.G.d. Muro, L. Lezama, M. Insausti, T. Rojo, Polyhedron 2 (2004) 28.
[18] T.V. Yilmaz, E. Senel, C. Kazak, Solid State Sci. 6 (2004) 859.
[19] J.L.C. Rowsel, O.M. Yaghi, Microporous Mesoporous Mater. 73 (2004) 3.
[20] D.J. Chesnut, D. Hagrman, P.J. Zapf, R.P. Hammond, R. LaDuca, R.C. Haushalter, J. Zubieta, Coord. Chem. Rev. 192 (1999) 737.
[21] Q. Yue, J. Yang, G.H. Li, G.D. Li, W. Xu, J.S. Chen, S.N. Wang, Inorg. Chem. 44 (2005) 5241.
[22] M. Eddaoudi, D.B. Moler, H.L. Li, B.L. Chen, T.M. Reineke, M. O'Keeffe, O.M. Yaghi, Acc. Chem. Res. 34 (2001) 319.
[23] T. Devic, C. Serre, N. Audebrand, J. Marrot, G. Ferey, J. Am. Chem. Soc. 127 (2005) 12788–12789.
[24] P. Angerer, L.G. Yu, K.A. Khor, G. Korb, I. Zalite, J. Eur. Ceram. Soc. 25 (2005) 1919.
[25] G.B. Deacon, R.J. Phillips, Coord. Chem. Rev. 33 (1980) 227.
[26] K. Nakamoto (Ed.) Wiley, New York, 1986.
[27] A. Seguatni, M. Fakhfakh, N. Jouini, Solid State Sci. 7 (2005) 1272.
[28] B. Mavis, M. Akinc, Chem. Mater. 18 (2006) 5317.
[29] P. Blaha, K. Schwarz, P. NovaK, Int. J. Quantum Chem. 101 (2005) 550.
[30] M. Kinyanjui, P. Axmann, M. Wohlfart-Mehrens, P. Moreau, F. Boucher, U. Kaiser, J. Phys.: Condens. Matter 22 (2010) 275501.
[31] K.L. Yao, J.Q. Zhang, Z.L. Liu, G.Y. Gao, Y.L. Li, D. Xi, Q. Ning, J. Magn. Magn. Mater. 320 (2008) 458.